Symbolic Dynamics and Pruning Fronts for the Stadium Billiard

Predrag Cvitanović
Center for Chaos and Turbulence Studies, Niels Bohr Institute,
Blegdamsvej 17, DK-2100 Copenhagen Ø, Denmark
and
Kai T. Hansen*
Fakultät für Physik, Universität Freiburg
Hermann-Herder-Strasse 3, D-79104 Freiburg, Germany
e-mail: k.t.hansen@fys.uio.no

September 4, 1995

[1]

Abstract

We construct a C_{2v} symmetry invariant symbolic dynamics for the Bunimovich stadium which is, in the limit of infinitely long stadium, a subshift of finite type. For any given finite length stadium we determine the inadmissible symbol sequences by means of a pruning front.

1 Introduction

The key to analysis of dynamics of a chaotic system is good symbolic dynamics; in particular, enumeration of admissible orbits is a prerequisite to any application of the periodic orbit theory[1, 2, 3]. For 1-dimensional mappings the kneading theory of Milnor and Thurston[4]

*Also at: Physics Department, University of Oslo, Box 1048, Blindern, N-0316 Oslo, Norway.

[1] **revised version, file:**
kompleks.nbi.dk:/home/cmplx/predrag/articles/stadium/stadium5.tex
Ascona proceedings, Ascona proceedings, submitted to J Stat Phys, 15 nov 1994.
This is the rewritten and resubmitted version 16 jul 1994

yields a complete description of admissible orbits of unimodal maps. For hyperbolic 2-dimensional maps and 3-dimensional flows it has been conjectured that all admissible orbits are given by means of the appropriately constructed *pruning fronts* [5, 6], 2-dimensional generalizations of Milnor-Thurston kneading sequences. The theory is relatively easy to implement for piecewise monotone dynamical systems such as the Lozi map[10, 5] and dispersing billiards[8, 9], where turnback or other singular points play a role analogous to the critical points in 1 dimension. In one case, a family of Lozi maps, the existence of the pruning front is no longer a conjecture, as it has been recently rigorously established by Ishii[7].

In this paper we carry out the pruning front construction for the Bunimovich stadium[11]. While the stadium billiard is one of the most commonly used examples of an ergodic dynamical system, its symbolic dynamics is more complicated than that of other systems analyzed in detail in literature, such as the n-disk pinballs and the Hénon map. Some systems, such as the Smale horseshoe[14], the well separated 3-disk pinball[15], and the cat map[16] have simple Markov partitions, but for generic ergodic billiards it has been proved by Sinai, Bunimovich and others[17, 18, 19] that there exist infinite but countable Markov partitions. Such systems can be approximated by more and more refined finite Markov partitions, and correspondingly more and more complicated symbolic dynamics. Nevertheless, it is possible to obtain useful finite approximations to the symbolic dynamics, and guarantee that all periodic orbits up to given length have been taken into account. One variant of covering symbolic dynamics has in this case already been constructed by Biham and Kvale[12]. We construct a different symbolic dynamics following the approach of ref. [21], and obtain two main new results: (1) a complete Markov partition for the symmetry reduced infinitely long stadium, and (2) a pruning front that gives the *exact* description of all admissible orbits for finite length stadia in the same sense in which the kneading theory accomplishes this task for the unimodal maps.

PC: Kai, can you enter the refernces the referees want here?

The paper is organized as follows: In sect. 2 we construct a desymmetrized covering symbolic dynamics for a stadium of infinite length. In sect. 7 we describe the stable/unstable manifold structure for the stadium billiard. In sect. 5 we relate this symbolic dynamics to Markov partitions of the phase space, and in sect. 6 we use the topology of such Markov partitions to construct a topologically faithful symbol plane representation of the dynamics. This enables us to construct the exact pruning front for a given finite length stadium in sect. 7. We then show how these pruning fronts can be approximated by finite

PC: fix up this list when done

grammar cycle expansions, and apply these to estimate the topological entropy of a finite length stadium.

2 Stadium symbolic dynamics

The stadium is a plane billiard whose border consists of two *semicircles* of radius 1 connected by two straight *sidewalls* of length $2a$, where a is the only parameter in the problem. A point particle moves freely within this two dimensional domain and is reflected elastically off the border. The dynamics is invariant under under the x_1 and x_2-axis reflections σ_1, σ_2, where the x_1-axis goes through the centers of the semicircles, and the x_2-axis bisects the stadium. The σ_1 and σ_2 together generate the symmetry group C_{2v} with 4 group elements $\{e, \sigma_1, \sigma_2, \sigma_1\sigma_2\}$. The curvature of the border changes discontinuously at the point where a sidewall joins the semicircle; this point (together with its 3 symmetric images) is the the only *singular point* on the border.

The *desymmetrized* symbolic dynamics[21] that we implement here labels trajectories by types of transitions between bounces, rather than by labeling segments of the stadium wall (as is done, for example, in ref. [12]). For dynamical systems with a symmetry - in this case the C_{2v} symmetry group generated by reflections across the two symmetry axes - such symbol sequences are invariant under the symmetry group transformations, and reduce the global dynamics to dynamics in the fundamental domain. Desymmetrization factorizes and simplifies the associated zeta functions and Fredholm determinants, and greatly improves convergence of computations over chaotic sets[21].

A *covering* symbolic dynamics has to account for all possible orbits, including those which exist for a sufficiently long stadium, but not necessarily for small a. We start by constructing the covering dynamics for the "unfolded" stadium.

2.1 Unfolded stadium

If bounces off the stadium side walls are elastic, they have no effect on the stability of the trajectory other than a factor (-1) per bounce, and the dynamics is conveniently visualized in the *unfolded stadium*, Fig. 1, in which n consecutive stadium sidewall bounces correspond to a free flight across n stadium tiles. The covering symbolic dynamics for an unfolded stadium is exceedingly simple: a trajectory that leaves a given semicircle crosses S_1 tiles before hitting the next semicircle,

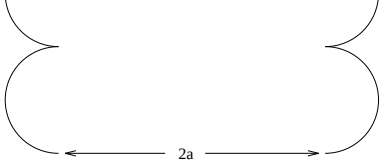

Figure 1: The unfolded stadium. A trajectory segment consists of free flight across S_i tiles (in the drawing the trajectory advances 2 tiles), followed by a clockwise or anticlockwise rotation by R_i steps within a semicircle.

bounces R_1 times around that semicircle, crosses S_2 tiles to the next bounce, and so forth. As the unfolded stadium is translationally symmetric, the initial semicircle need not be specified, and the bi-infinite itinerary

$$\cdots S_{-1}R_{-1}S_0R_0 \cdot S_1R_1S_2R_2S_3R_3 \cdots$$

specifies the trajectory. This symbolic dynamics is natural in the sense that it is in one-to-one correspondence with the factorization of the Jacobian matrix of the trajectory, and it captures the intermittency effects induced by the existence of the "bouncing ball" and "whispering gallery" orbits (see sect. 8.2).

As the unfolded stadium is symmetric under reflection across the the x_2 axis, it is convenient to exploit this symmetry before proceeding with the partitioning of the phase space.

2.2 Unfolded 1/2 stadium

We shall desymmetrize the symbolic dynamics in two steps. Consider first the C_v symmetry corresponding to the σ_2 reflection that maps the opposite semicircles into each other, and define the *fundamental domain* as the $x_1 \geq 0$ unfolded 1/2 stadium. A global trajectory is reduced to the fundamental domain trajectory by reflecting its $x < 0$ segments across the x_2-symmetry axis. Hence every fundamental do-

main trajectory that does not traverse a singular point can be labeled by a bi-infinite itinerary

$$\cdots S_{-1}R_{-1}S_0R_0 \cdot S_1R_1S_2R_2S_3R_3 \cdots$$

where the i-th symbol pair refers to a semicircle *rotation* R_i followed by a tile *translation* S_i:

$$R_i = \begin{cases} \rho_1, \rho_2, \rho_3, \cdots & \text{rotate clockwise 1, 2, 3, ... steps} \\ \rho_0 & \text{reflect out in one bounce} \\ \rho_{-1}, \rho_{-2}, \rho_{-3}, \cdots & \text{rotate anticlockwise 1, 2, 3, ... steps} \end{cases}$$

$$S_i = \begin{cases} \alpha_1, \alpha_2, \alpha_3, \cdots & \text{ascend the } x_2\text{-axis} \\ \alpha_0 & \text{remain in the tile} \\ \alpha_{-1}, \alpha_{-2}, \alpha_{-3}, \cdots & \text{descend the } x_2\text{-axis} \end{cases} \tag{1}$$

Time reversal maps $\{\alpha_i, \rho_i\} \to \{\alpha_{-i}, \rho_{-i}\}$. Every translation α_i carries a factor σ_2 (we need this to keep track of the spatial ordering of partitions, sect. 4).

C_v symmetric unfolded stadia might be of interest in their own right as models of deterministic transport and diffusion, realizable experimentally in 2-d electron gas nanostructures. Analogous construction yields a symbolic dynamics for a C_2 symmetric unfolded stadium, describing, for example, the motion of a charged particle in a magnetic field perpendicular to the plane of the stadium.

2.3 Unfolded 1/4 stadium

The stadium considered here is also symmetric with respect to the σ_1 reflection across the x_1-axis. The σ_1 symmetry can be used to turn any given rotation subsequence and any given free flight segment into the canonical direction. We take as the fundamental domain the upper right unfolded 1/4 stadium, $x_1 > 0, x_2 > 0$, and orient the trajectory so that its i-th rotation segment consists of one or more clockwise bounces along the right semicircle. The trajectory exits the right end half-disk in the upper right quadrant and crosses over to the opposite half-disk, or ascends $1, 2, 3, \ldots$ tiles, either directly, or after a σ_1 reflection. The sense of next rotation depends on whether the trajectory enters the next semicircle below or above the semicircle center; so we have to distinguish the trajectories that cross even number of center-to-center lines between the i-th and $(i+1)$-th stadium end half-disks, and those that cross odd numer of times. Hence the symbolic

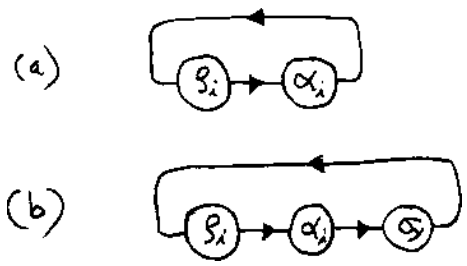

Figure 2: (a) Markov diagram for the unfolded stadium, no symmetry, $a \to \infty$. (b) Markov diagram for the C_{2v} unfolded 1/2 stadium symbolic dynamics, $a \to \infty$, Eq. (1).

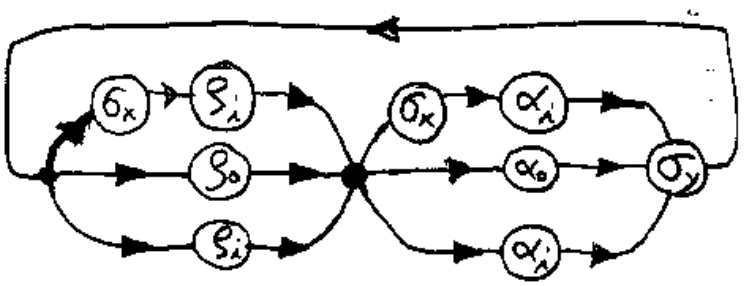

Figure 3: Markov diagram for the C_{2v} unfolded 1/4 stadium (2), $i = 1, 2, 3, \cdots$.

dynamics appropriate to the C_{2v} symmetric stadium is

$$R_i = \begin{cases} \rho_1, \rho_2, \rho_3, \cdots & \text{rotate 1, 2, 3, ... steps} \\ \rho_0 & \text{bounce out} \\ \rho_{\underline{1}}, \rho_{\underline{2}}, \rho_{\underline{3}}, \cdots & \sigma_1, \text{ then rotate 1, 2, 3, ... steps} \end{cases}$$

$$S_i = \begin{cases} \alpha_1, \alpha_2, \alpha_3, \cdots & \text{ascend the } y\text{-axis} \\ \alpha_0 & \text{remain in the tile} \\ \alpha_{\underline{1}}, \alpha_{\underline{2}}, \alpha_{\underline{3}}, \cdots & \sigma_1, \text{ then ascend the } y\text{-axis} \end{cases} \tag{2}$$

Every bi-infinite sequence corresponds to an orbit in the fundamental domain, in this case the unfolded 1/4 stadium.

PC: fix this: Examples of the unfolded 1/4 stadium periodic orbits are given in Fig. 4.

3 Unfolded stadium phase space

The symbolic dynamics partitions the unfolded stadium phase space as follows. The convenient Poincaré section is the flat face of the end half-disk, Fig. 5. For a given x the outgoing trajectory sweeps

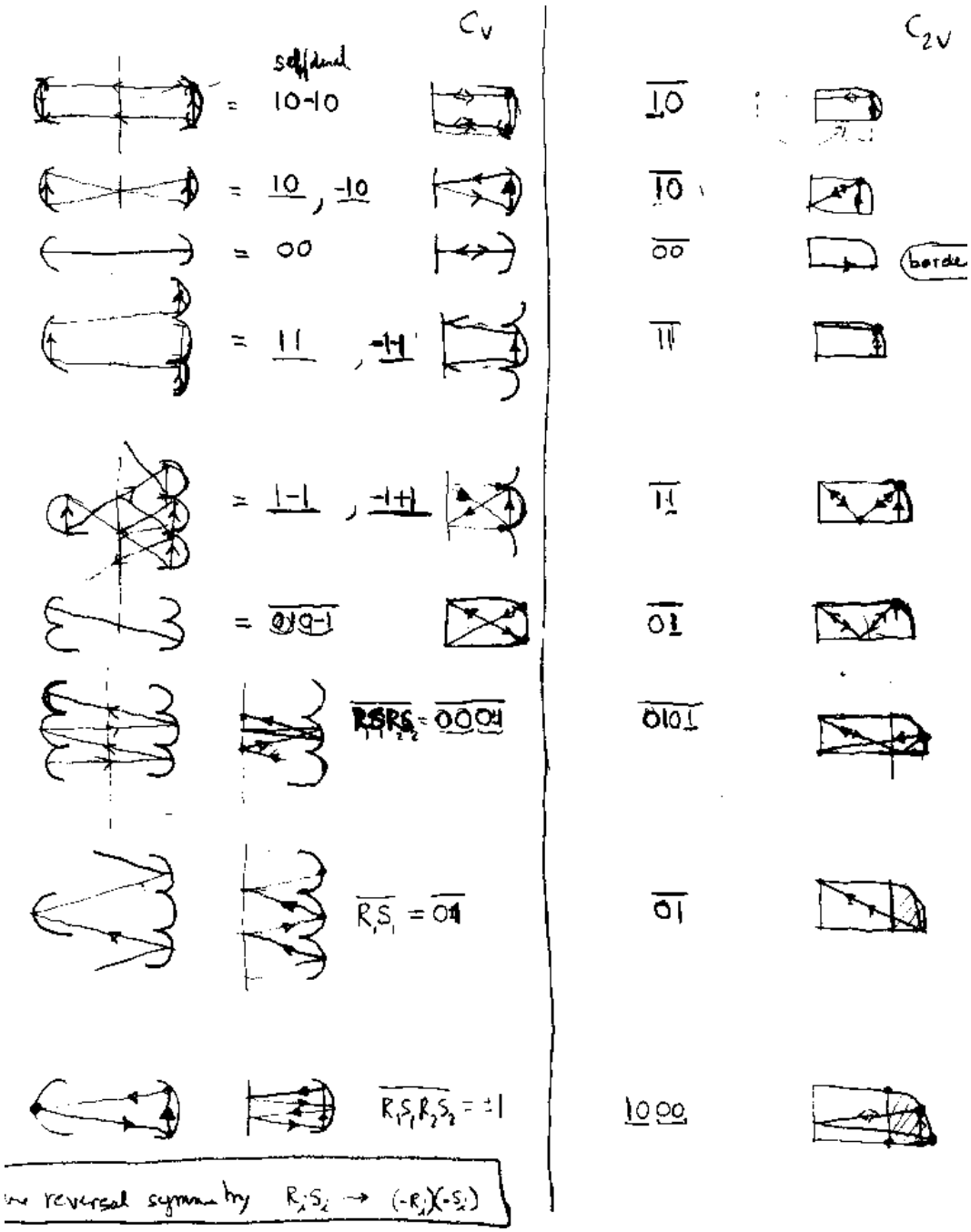

Figure 4: Examples of the periodic orbits for the unfolded stadium, the unfolded 1/2 stadium together with the corresponding periodic orbits for the 1/4 stadium.

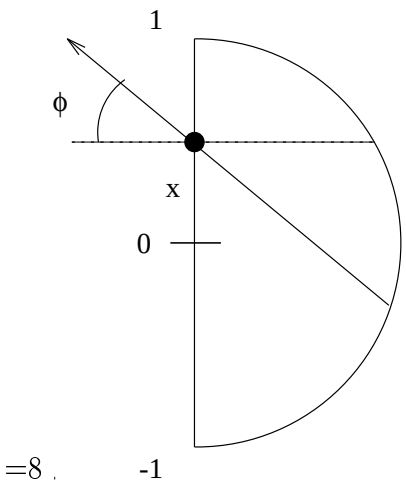

Figure 5: Definition of the half-disk Poincaré section $(x, \sin\phi)$, $\cos\phi > 0$, where $x \in [-1, 1]$ and $\sin\phi = p_x$ is the moment component parallel to the x axis.

through the phase space strips $S_1 \in \{\cdots \alpha_{-1}, \alpha_0, \alpha_1, \alpha_2, \cdots\}$ corresponding to translations by $\cdots, -1, 0, 1, 2, \cdots$, Fig. 6. At the same time the ingoing trajectory sweeps through phase space rings $R_0 \in \{\cdots \rho_{-1}, \rho_0, \rho_1, \rho_2, \cdots\}$ corresponding to $\cdots, -1, 0, 1, 2, \cdots$ clockwise rotation steps along the semicircle, Fig. 7. The partition lines in Fig. 6 and Fig. 7 are given by

$$\begin{aligned} \sin\phi &= \sin\left(\arctan\left(\frac{1-x+2k}{2a}\right)\right), \quad k \in Z \\ x &= \sin(\pi/2 - \alpha/2)/\sin(-\pi/2 + \alpha(k+1/2)) \\ \sin\phi &= \sin(\pi - \alpha(k+1/2)), \quad k \in N \end{aligned} \tag{3}$$

Together, the two sets of boundaries partition the phase space into "rectangles" $[R_0.S_1]$. The dot in $[R_0.S_1]$ indicates the present instant.

PC: Kai, can you recheck, explain these? What is α?

PC: explain that future = configuration partition, past = momentum partition. Baker's map is like that as well (Saraceno).

In the infinitely thin billiard limit $a \to \infty$ every S_i strip intersects transversally every R_j strip, and the $\{R_i S_i\}$ symbolic dynamics is unrestricted. For finite a this symbolic dynamics is pruned, as long rotation sequences ($|R_i|$ large) cannot be followed by long free flights ($|S_i|$ large). The reason is is clear by inspection of Fig. 5; a long rotation sequence requires the grazing incidence angle $\to \pm 0$, while a long flight requires nearly perpendicular incidence angle $\to \pi/2$, and for any finite stadium length a the two conditions are incompatible. The *admissible* itineraries will be determined in sect. 7. That one and only one symbol sequence corresponds to a given admissible trajectory

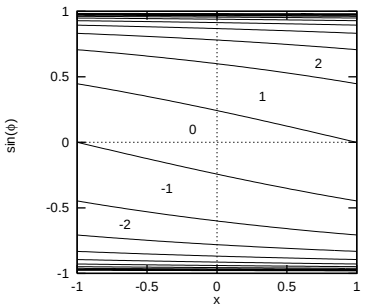

Figure 6: One step into the future the phase space is partitioned into strips $S_1 \in \{\cdots \alpha_{-1}, \alpha_0, \alpha_1, \alpha_2, \cdots\}$ by boundaries $(x, \sin\phi) \to B_i$ which correspond the orbits that end in the i-th translation of the singular point B. In this example the billiard lenght parameter is $a = 1$.

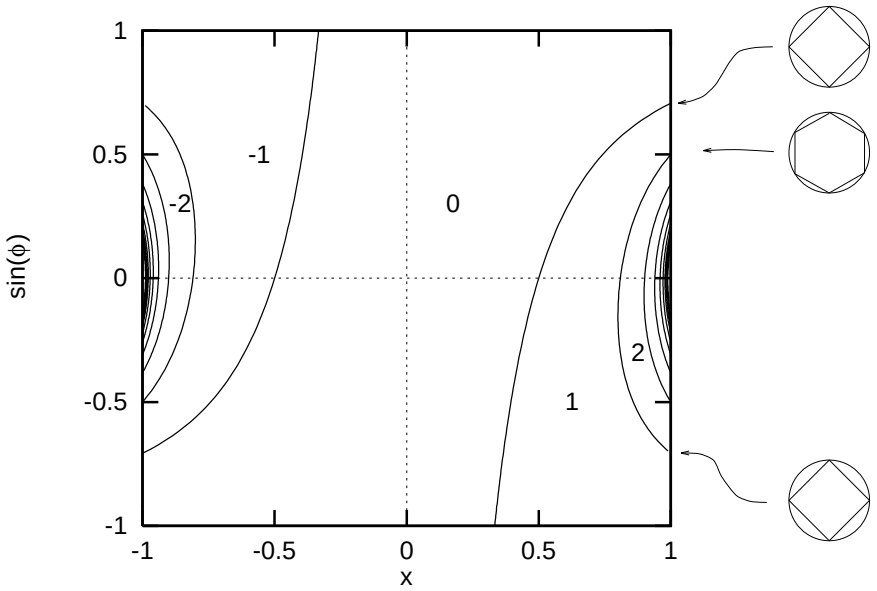

Figure 7: One step into the past the phase space is partitioned into strips $R_0 \in \{\cdots \rho_{-1}, \rho_0, \rho_1, \rho_2, \cdots\}$ by boundaries $B \to (x, \sin\phi)$ which correspond the orbits that originate at the edge singular point B and reach the Poincaré section after $|\rho_i| + 1$ bounces along the semicircle. On the $\sin\phi = 0$ and $x = \pm 1$ lines the boundary trajectories correspond to regular polygons inscribed into the circle. Overlayed on the forward partition Fig. 6, the two sets of boundaries partition the phase space into "rectangles" $[R_0.S_1]$.

follows by standard arguments for hyperbolic systems, see for example refs. [13, 20].

4 Unfolded stadium symbol plane

We now construct a topologically faithful symbol plane representation of the the above unfolded stadium phase space partion. The idea is very simple: For a hyperbolic system a rectangle $[s_{-m}\cdots s_0.s_1\cdots s_n]$ is the intersection of the finite future itinerary strip $[.s_1 s_2\cdots s_n]$ with the finite past itinerary strip $[s_{-m}\cdots s_{-1}s_0.]$. The symbol plane that we shall now construct is a topologically conjugate representation of the stable/unstable manifolds foliation, with the manifolds straightened out into a "street map".

We start by turning the above symbolic dynamics into a topologically *well-ordered* alphabet such that the natural ordering of symbol strings corresponds to the topological ordering of orbits in the Poincaré plane. We do this by replacing the symbols R_i and S_i with the integers used as index in (1), and reversing the signs of symbols following every free flight, as the reflection off the straight x_2 wall reverses the ordering of the symbols. Define $\overline{S}$, $\overline{R}$ by:
If $S_k = \alpha_j$, then $\overline{S}_k = \alpha_{-j}$
If $R_k = \rho_j$, then $\overline{R}_k = \rho_{-j}$

The new symbol string is then given as

$$\{w_i\} = \cdots \overline{R}_{-3}\overline{S}_{-2}R{-}2S_{-1}\overline{R}_{-1}\overline{S}_0 R_0 \cdot S_1\overline{R}_1\overline{S}_2 R_2 S_3\overline{R}_3 - \overline{S}_4\cdots$$

We can now determine a symbolic coordinate space (γ,δ) by defining γ (the symbolic future) to be the limit value of γ_n for $n\to\infty$ given by the algorithm

$$\begin{aligned}
\gamma_n &= \gamma_{n-1} + \Delta_{n-1}\times\left\{\begin{array}{ll} \frac{1}{3}b^{|w_n|} & \text{if } w_n<0 \\ \frac{1}{3} & \text{if } w_n=0 \\ 1-\frac{1}{3}b^{w_n-1} & \text{if } w_n>0 \end{array}\right\} \\
\Delta_n &= \Delta_{n-1}\times\left\{\begin{array}{ll} \frac{1}{3}(b^{|w_n|-1}-b^{|w_n|}) & \text{if } w_n<0 \\ \frac{1}{3} & \text{if } w_n=0 \\ \frac{1}{3}(b^{w_n}-b^{w_n-1}) & \text{if } w_n>0 \end{array}\right\}
\end{aligned} \tag{4}$$

with $\gamma_0 = 0$ and $\delta_0 = 1$, and δ (symbolic past) in a similar way for negative n. We have chosen $b = 1/2$. [2]

[2] KTH: or if you want 1/4

PC: to be consistent we should use here Gauss map style $1/w_n$ rather than the exponentially shrinking b^{w_n} here!

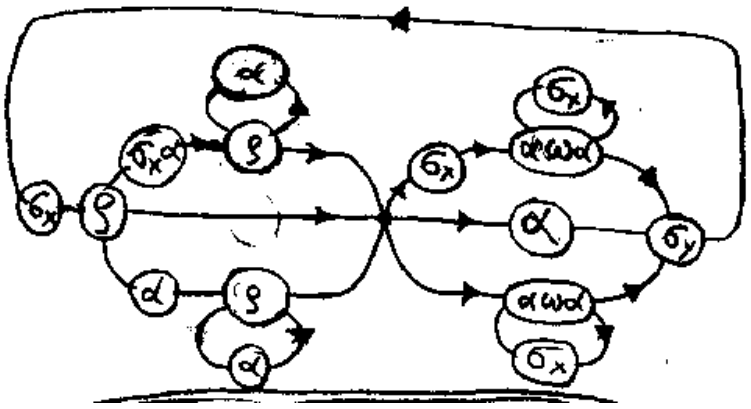

Figure 8: Markov diagram for the C_{2v} symmetric 1/4 stadium, 1-step symbolic dynamics.

5 1/4 stadium Markov graph

We now rewrite the above infinite alphabet symbolic dynamics as a 1-step dynamics appropriate to describing a motion confined to the C_{2v} symmetry fundamental domain, the 1/4 stadium. This is necessary if one insists on describing the dynamics by a finite alphabet, or if the quantity of interest depends on bounces off flat walls. Such situations arise if collisions are inelastic, or if one is computing a quantity such as the pressure exerted on the billiard walls by an elastically bouncing particle.

The bi-infinite alphabet of sect. 2.3 is truncated to a 1-step alphabet by keeping only $R_i \in \{\rho_{\underline{1}}, \rho_0, \rho_1\}$, $S_i \in \{\alpha_{\underline{1}}, \alpha_0, \alpha_1\}$, and accounting for rotation sequences $|R_i| > 1$ and repeated sidewall bounces $|S_i| > 1$ by repeats of the 1-step symbols. As in the repeated rotations and translations the sense is preserved for the duration of the sequence, the 1-step symbolic dynamics has memory which can be encoded in a Markov graph.

Putting all this together, we obtain the 3-node Markov graph of Fig. 9, with the 11-letter alphabet $s_t \in \{a, b, c, d, \ldots, k\}$ labeling paths from one node to the next. There can be several topologically distinct paths connecting a pair of nodes.

The Markov graph consists of 3 nodes, corresponding to bounces either off the sidewall (I), off the semicircle as a first bounce in the semicircle (II), or off the semicircle as a second or later bounce (III).

Each of the three nodes of the Markov diagram of Fig. 9 corresponds to a partition of the associated part of the phase space. This partition is obtained by letting the arrows into and out from the node

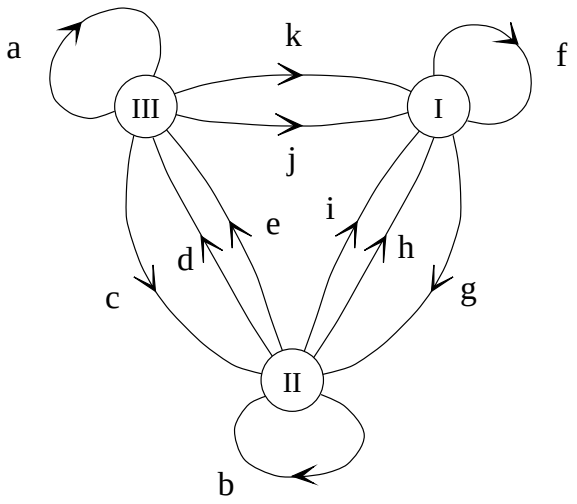

Figure 9: The Markov graph for the $a \to \infty$ infinite length $1/4$ stadium with 11-letter alphabet $s_t \in \{a, b, c, \ldots, k\}$.

define an area in the phase space which we shall call a *rectangle*. For example, the rectangle $[s_0.s_1 s_2]$ includes all orbits whose itinerary includes a subsequence $\cdots s_0.s_1 s_2 \cdots$.

PC: Examples of the 1/4 stadium periodic orbits are given in Fig. 4.

A finite walk on a Markov graph partitions the phase space into sets of trajectories that traverse the phase space in the prescribed order; longer and longer symbol sequences lead to finer and finer partitioning of the phase space. The Markov graph tells us what partitions exist at a given level of resolution; now we have to determine their relative ordering.

6 1/4 stadium symbol plane

PC: Need to explain that this is NEW; first example of a symbol plane constructed for a nontrivial subshift, with hierarchical partition with number of partitions depending on the where one is; there are no "holes" in the symbol plane, and no "geometrical" rules.

PC: Kai, cite your own papers here, for which this applies

We now construct a topologically faithful symbol plane representation of each of the three phase spaces introduced above. The idea is illustrated by Fig. 15 and Fig. 16. What is novel here compared to the reference[5] is that the forward and backward walks on the Markov diagram generate a partition for which a number of subintervals changes from level to level. Furthermore, in contrast to the previously used symbolic dynamics for stadium[12] and other billiards [?!] our symbolic dynamics requires no "geometric" pruning rules, *ie.* the symbol plane has no "white" regions that correspond to symbol sequences that cannot occur for any value of a. By construction, any point belonging to any orbit existing for $a = \infty$ maps into the symbol plane square

(δ, γ), with $0 \leq \delta \leq 1$ and $0 \leq \gamma \leq 1$.

In Fig. 15 (a), (b) and (c) the first level of the partition is drawn in the (δ, γ) planes for the three phase spaces. The symbol plane is constructed by dividing the δ and γ axes into equal intervals for each in and out arrow from the nodes of Fig. 9, and ordering the symbol plane rectangles in the order of the corresponding phase spaces rectangles, Fig. 12, Fig. 13 and Fig. 14.

We then associate an integer v_t to each of the symbols, ordered as the corresponding rectangles in the (δ, γ) plane: $[.g] \to 0$ and $[.f] \to 1$ for the future and: $[j.] \to 0$, $[h.] \to 1$, $[h.] \to 2$, $[k.] \to 3$ and $[f.] \to 4$ for the past. This is the first step in constructing *well ordered* symbols; we denote the first future symbol by v_1, and the first past symbol by v_0.

Fig. 15 (b) and (c) shows the corresponding construction for the symbol planes II and III. The well ordered symbols v_t obtained from the symbols s_t for all three nodes are given in table 1. Note that a symbol s_t may correspond to a different symbol v_t, depending on whether it is a future or a past symbol.

The next level of partition is obtained by using the next partition of γ and δ from the node that one moves to (respectively came from) in Fig. 9. We illustrate this by an example.

Consider the rectangle $[j.f]$ in symbol plane I, Fig. 15 (a). All points in this rectangle correspond to a future symbol f. From the Markov graph Fig. 9 we find that f returns to node I and we therefore use the partition of γ of Fig. 15 (a). This yields the second level partition of γ into the two intervals $(1/2, 3/4)$ and $(3/4, 1)$. All points in the rectangle $[j.f]$ also correspond to a past symbol j, and Fig. 9 shows that the previous node was node III. The partition of δ is then made according to Fig. 15 (c) which yields three intervals $(0, 1/15)$, $(1/15, 2/15)$ and $(2/15, 1/5)$. The rectangle $[j.f]$ now splits into a second level partition of 6 rectangles, with the labeling of each rectangle given in Fig. 16 (a).

Note that the ordering of the past symbols $[aj.]$, $[dj.]$ and $[ej.]$ is reversed compared to Fig. 15 (c). If we analyze the second level partition of the rectangle $[k.f]$ which also comes from node III, we get three intervals along the δ-axis, but in this case the ordering of Fig. 15 (c) is preserved; $[ek.]$, $[dk.]$ and $[ak.]$. The first and second level of the partition of the whole symbol plane I are drawn in Fig. 16 (b).

Whether the arrow connecting the nodes in Fig. 9 implies order reversal or preservation has to be incoded in the construction of the symbol plane (δ, γ). It is easy to verify that for future symbols the

PC: This is buried too deep - must state reversal rules simply an clearly

PC: Kai, I think this will be all much simpler for the infinite alphabets - why don't you give it a try?

symbols c, d, h and k reverse the ordering, while e, h and j reverse the ordering for the past symbols. The remaining symbols preserve the ordering. The ordering can be reversed because bounces off the sidewall reverse the ordering of two neighboring orbits, while the bounces off the semicircles preserve the ordering.

We can now calculate the symbol plane coordinates (γ, δ) of any orbit given its itinerary. The algorithm for computing the values γ and δ is more complicated than for a simple horseshoe map[5] because here the symbol plane is partitioned into rectangles of different sizes (see Fig. 16 (b)).

Let $N_i^{\rm in}$ and $N_i^{\rm out}$ be the number of arrows into and out from the node i: $N_{\rm I}^{\rm in} = 5$, $N_{\rm I}^{\rm out} = 2$, $N_{\rm II}^{\rm in} = 3$, $N_{\rm II}^{\rm out} = 5$, $N_{\rm III}^{\rm in} = 3$ and $N_{\rm III}^{\rm out} = 4$. An orbit is specified by its itinerary $\cdots s_{-1}s_0.s_1s_2\cdots$. Let i_t be the node to which the arrow s_t arrives at for $t \leq 0$, or from which it leaves for $t > 0$. Let $V^- = \cdots v_{-2}v_{-1}v_0$ be given by the past values v from Table 1 obtained from the symbols $\cdots s_{-2}s_{-1}s_0$, and $V^+ = v_1v_2v_3\cdots$ be given by the future values v obtained from the symbols $s_1s_2s_3\cdots$.

The "past" coordinate δ is given by $\delta = \lim_{t\to-\infty} \delta_t$, where δ_t with $t \leq 1$ is computed iteratively by

$$\begin{aligned}
m_{t-1} &= m_t/N_{i_{t-1}}^{\rm in}\,, && m_1 = 1 \\
p_{t-1} &= \begin{cases} p_t & \text{if} \quad s_t \in \{a,b,c,d,f,g,i,k\} \\ -p_t & \text{if} \quad s_t \in \{e,h,j\} \end{cases}, && p_0 = 1 \\
\delta_{t-1} &= \delta_t + \begin{cases} v_{t-1}m_{t-1} & \text{if} \quad p_{t-1} = 1 \\ (N_{i_{t-1}}^{\rm in} - 1 - v_{t-1})m_{t-1} & \text{if} \quad p_{t-1} = -1 \end{cases}, && \delta_1 = 0\,.
\end{aligned} \tag{5}$$

The "future" coordinate γ is given by $\gamma = \lim_{t\to\infty} \gamma_t$ where γ_t with $t \geq 0$ is computed iteratively by

$$\begin{aligned}
m_{t+1} &= m_t/N_{i_{t+1}}^{\rm out}\,, && m_0 = 1 \\
p_{t+1} &= \begin{cases} p_t & \text{if} \quad s_t \in \{a,b,e,f,g,i,j\} \\ -p_t & \text{if} \quad s_t \in \{c,d,h,k\} \end{cases}, && p_1 = 1 \\
\gamma_{t+1} &= \gamma_t + \begin{cases} v_{t+1}m_{t+1} & \text{if} \quad p_{t+1} = 1 \\ (N_{i_{t+1}}^{\rm out} - 1 - v_{t+1})m_{t+1} & \text{if} \quad p_{t+1} = -1 \end{cases}, && \delta_0 = 0\,.
\end{aligned} \tag{6}$$

7 The pruning front

The trajectories that hit the singular points are the 2-d analogues of the unimodal map critical point trajectory, and play the key role in our generalization of the Milnor-Thurston kneading theory to 2-d billiards.

Typical structure of the stadium stable/unstable manifolds is illustrated by the unstable period-2 cycle manifolds at $a = 1$ drawn in

Fig. 11. The manifolds consists of smooth sections bracketed by sharp kinks, the *turning points*. A turning point is created whenever the evolution sweeps a manifold across the singular point on the boundary, as the derivative of the reflection of point particle is discontinuous at the singular point.

Intersections of the stable and the unstable manifolds (see Fig. 11 (c) and (d)) are transverse and dense in the phase space. As a, the length of the stadium decreases, the manifolds move in such a way that infinite families of the stable/unstable manifolds intersections are lost. This occurs at points where a smooth section of the stable manifold touches a turning point of the unstable manifold (the analogue of a homoclinic tangency for a smooth diffeomorphism). Any finite change of the parameter a sweeps through bifurcations of an infinite number of periodic orbits, but no stable orbits occur, very much as in the case of the Lozi map[5] whose stable/unstable manifolds also have sharp turning points.

We are now finally in position to draw the pruning front and determine the inadmissible orbits for a given finite length stadium. This way of describing symbolic dynamics of 2-d hyperbolic systems was introduced for the Lozi and Hénon maps in refs. [5, 6], and applied to dispersive billiards in ref. [9]. Here we give for the first time a construction of the pruning front for a focusing billiard. The singular point on the border determines whether a given symbol sequence corresponds to an admissible orbit. All orbits which are pruned as the stadium length decreases disappear as a bounce in the orbit hits the singular point.

Our strategy is to single out one family of turning points which we call the *primary* turning points; this family is the stadium billiard's analogue of the critical point of a unimodal mapping. All other turning points are images or pre-images of the primary ones. We then map the primary turning points into a symbol plane (defined below), and construct the *pruning front* by connecting this set of points into a monotone boundary line. The area on one side of the pruning front corresponds to symbol sequences that are inadmissible for the given finite length stadium. These sequences are "pruned"; what remains is the set of all admissible symbol sequences for the system.

The pruning front is constructed by scanning through all orbits starting (or ending) at the singular point at different angles, and mapping the corresponding future and past symbol sequences into the symbol planes I, II and III by algorithms (5) and (6). The resulting pruning fronts, Figs. 17, 18 and 19, are fractal sets of points in the (δ, γ) plane. The pruning front is monotone in the since the symbol

plane is constructed with well ordered symbols which respect the foliation of the stable/unstable manifolds, so the points can be connected by any monotonically increasing or decreasing line, and the area outside the pruning front, the primary forbidden region, contains points corresponding to all inadmissible orbits. In Fig. 20 points belonging to several long chaotic orbits are plotted in the symbol plane I; as expected, the pruning front in Fig. 17 is the border between these points and the primary forbidden region. The white regions in such figures correspond to the forbidden symbol sequences, but one needs to define only the *primary* forbidden regions as all other (white) regions are either images or preimages of these.

The primary forbidden region is rather small for $a = 5$. It increases with decreasing a and is already quite large for $a = 0.5$, see Fig. 20. In the integrable limit $a \to 0$ only the rotation orbits existing in the circle survive[27].

We now approximate the pruning front by partitioning the symbol plane into an integer lattice, and tracing out approximate pruning fronts along the lattice lines of this partition. In Fig. 21 the symbol plane I partition lines of the first and second level are drawn together with the pruning front. The rectangles completely in the primary forbidden regions are shaded and correspond to the symbol substrings $[j.f]$, $[f.gd]$, $[aj.ge]$, $[gh.ff]$, $[ch.ff]$, $[kf.gh]$, $[ff.gh]$ and $[ak.gd]$. From the other symbol planes we get further forbidden substrings: all completely forbidden substrings up to length 4 are

$$\begin{aligned} &jf,\ ak \\ &fgd,\ gea \\ &ajge,\ ghff,\ chff,\ kfgh,\ ffgh,\ cdkf,\ gdkf,\ aace,\ acea,\ kgej,\ fgej. \end{aligned} \tag{7}$$

Given such list we can construct a Markov diagram which generates all admissible orbits in this approximation. As only the fully pruned rectangles have been removed, this approximation underestimates the number of pruned orbits.

8 Dynamical zeta functions

The above Markov diagrams can be applied to calculating averages and spectra of classical and quantum mechanical systems. Each fundamental domain periodic orbit corresponds to a segment of periodic orbit of the full stadium problem. The weights with which such periodic orbits contribute to factorized zeta functions for the irreducible representations of C_{2v} are given in ref. [21], sect. 7.4. Here we shall

Figure 10: The Markov graph as in Fig. 9, but approximating $a = 1$ finite $1/4$ stadium symbolic dynamics, with the length-2 strings $_jf_$, $_ak_$ of the pruning list (7) forbidden.

restrict our considerations to the fully symmetric A_1 representation for which all group theory weights equal 1.

To illustrate such applications, we briefly outline a calculation of the topological entropy h (for the finite alphabet of sect. 5) and the metric entropy K (for the infinite alphabet of sect. 2.3) .

8.1 Topological entropy

The topological entropy is a measure of how fast the number of periodic orbits grows as the cycle length increases. The number of periodic orbits with symbol string length l in the limit $l \to \infty$ is given by $N(l) \sim e^{hl}$, where the value of h is given by the logarithm of the inverse of the smallest zero of the topological zeta function[22].

For a finite Markov graph the topological zeta function is given by the characteristic polynomial of the graph. The characteristic polynomial is obtained by counting the number of non-self intersecting closed paths on the graph, and combinations of such closed paths without common nodes[6].

The characteristic polynomial for the $a = \infty$ Markov graph of Fig. 9 is

$$1/\zeta_{\rm top}(z) = 1 - 3z - z^2 - z^3 \,, \tag{8}$$

with leading eigenvalue $z = e^h$,

$$h = \ln 3.38298\ldots = 1.21875\ldots \tag{9}$$

This is the upper bound on the topological entropy of any stadium billiard. The Markov diagram for two forbidden strings of length 2 approximation to the $a = 1$ symbolic dynamics, Fig. 10 yields

$$1/\zeta_{\rm top}(z) = 1 - 3z - z^2 - z^3 + 4z^4$$

with the slightly smaller topological entropy

$$h = \ln 3.28428\ldots = 1.18915\ldots$$

The Markov diagram with the four forbidden strings of lengths 2 and 3 from the list (7) yields

$$1/\zeta_{\rm top}(z) = 1 - 3z - 3z^3 + 5z^4 + 2z^5 + 6z^6 + z^7$$

with topological entropy

$$h = \ln 3.10061\ldots = 1.131600\ldots$$

For comparison, the numbers of periodic points listed in the table I of ref. [12] for the $a = 1.6$ yields $h \approx 1.1$.

As more and more forbidden sequences are taken into account, the construction of topological zeta functions becomes more laborious, but not impossible. The most detailed evaluation of topological entropy from a pruning front has been implemented by Grassberger *et al.*[23] for the Hénon attractor. We do not pursue such calculation here. The reason is that while in the case of almost purely hyperbolic systems such as the Hénon attractors and repellers, organization of cycles by finite alphabet symbolic dynamics also reflects their relative importance in evaluation of chaotic averages, for nonhyperbolic systems such as the stadium the finite alphabet symbolic dynamics does not account for the intermittency effects.

8.2 Intermittency

Infinite alphabets are a typical feature of systems with intermittency, the simplest and most studied example being the Farey and the Gauss maps[24, 25, 26]. When a symbolic dynamics alphabet has infinite range, it clearly makes no sense to talk about topological entropy, the rate of growth of admissible symbol strings with increase in the symbol string length: a meaningful measurment is the Kolmogorov or metric entropy, the rate of growth of admissible symbol strings weighted by the natural measure. In the periodic orbit theory implementing this requires evaluation of the cycle stability eigenvalues, with the periodic orbit weight $\approx \ln|\Lambda_p|/|\Lambda_p|$, where $|\Lambda_p|$ is the product of expanding eigenvalues of the cycle p Jacobian matrix[25].

PC: Kai, can you try to recheck this - it is pretty trivial, if one follows my lecture notes on billiard stability...

Motion in the unfolded billiard is intercalation of two integrable motions, stability of each of which is known analytically. The Jacobian matrix for $r = |R_k| + 1$ trajectory rotation segment contained within a semicircle is given by

$$\mathbf{J}_{R_k} = (-1)^r \begin{bmatrix} 1+2r & -2r\cos\phi_k \\ 2r/\cos\phi_k & 1-2r \end{bmatrix}, \qquad |R_k| > 0\,,$$

where ϕ_k is the outgoing angle to the normal, and the curvature radius equals -1 for our definition of the stadium. The single bounce and the free flight Jacobian matrix is

$$\mathbf{J}_{S_k} = (-1) \begin{bmatrix} 1 & 0 \\ -2/\cos\phi_k & 1 \end{bmatrix}, \qquad \mathbf{J}R_k|_{R_k=0} = \begin{bmatrix} 1 & \tau_k \\ 0 & 1 \end{bmatrix},$$

where τ_k is the length of the k-th free flight, roughly the number of traversed tiles, $\tau_k \approx |S_k|$. Hence the Jacobian matrix of a cycle p of length n_p is given by

$$\mathbf{J}_{S_1 R_1 S_2 R_2 \cdots S_{n_p} R_{n_p}} = \mathbf{J}_{R_{n_p}} \mathbf{J}_{S_{n_p}} \cdots \mathbf{J}_{R_2} \mathbf{J}_{S_2} \mathbf{J}_{R_1} \mathbf{J}_{S_1} \ . \tag{10}$$

Here existence of the "bouncing ball" family of infinite free flights induces families of periodic orbits of type $\overline{(\cdots)S}$, $S = \alpha_{\pm 1}, \alpha_{\pm 2}, \alpha_{\pm 3}, \cdots$, and existence of the creeping "whispering gallery" orbits that bounce infinitely many times around a semicircle induces families of periodic orbits of type $\overline{(\cdots)R}$, $R = \rho_{\pm 1}, \rho_{\pm 2}, \rho_{\pm 3}, \cdots$, whose stabilities fall off only as a power of $|S|$ (respectively $|R|$), rather than exponentially with the number of bounces. The billiard has two integrable limits, $a \to 0$ (pure rotation) and $a \to \infty$ (pure free flight), so the metric entropy (or the Lyapunov exponent) should vanish in these two limits, and be maximal somewhere inbetween. (The symbolic dynamics of the rotation orbits that survive in the $a \to 0$ limit has been studied by Meiss[27]). Controlling convergence of such algebraically decaying series is not easy, and as our focus here is on symbolic dynamics, these metric calculations are beyond the scope of this article and will be reported elsewhere.

9 Conclusions

We have introduced a symmetry reduced symbolics dynamics for the stadium billiard, obtained an exact description of all admissible orbits in terms of a pruning front, and shown how to construct approximate finite Markov partitions of the stadium phase space. The construction of the Markov graph for an infinitely long stadium and a pruning front for a finite length stadium are new results.

KTH gratefully acknowledges financial support by the A. von Humboldt Foundation and the Norwegian Research Council. PC was supported by the Carlsberg Fundation.

Note added to the revised version of the article: *Since the submission of this article we have received a preprint[20] from Akiyama and Koga. The authors do not desymmetrize the symbolic dynamics. They use an 18 letter alphabet which they apply to numerical estimation of the topological entropy (they obtain the same covering symbol dynamics upper bound (9)), and an equipartition vs. natural measure evaluation of the pressure. They do not discuss conditions on admissibility of itineraries.*

The original version of this article, preprint "Symbolic Dynamics and Markov Partitions for the Stadium Billiard", K.T. Hansen and P. Cvitanović, Los Alamos archive http://xyz.lanl.gov/nlin-sys/ chao-dyn/9502005, contains additional material, in particular the relation to the Biham-Kvale symbolic dynamics[12], omitted here for reasons of brevity.

References

[1] D. Ruelle, *Statistical Mechanics, Thermodynamic Formalism*, (Addison-Wesley, Reading MA, 1978).

[2] M.C. Gutzwiller, *Chaos in Classical and Quantum Mechanics* (Springer, New York 1990).

[3] P. Cvitanović, ed., *Periodic Orbit Theory - theme issue*, *CHAOS* **2**, 1-158 (1992).

[4] J. Milnor and W. Thurston, "On iterated maps of the interval", Ed. J.C. Alexander, *Lec. Notes in Math.* **1342,** 465 (Springer, Berlin, 1988).

[5] P. Cvitanović, G. H. Gunaratne, I. Procaccia, *Phys. Rev. A* **38**, 1503 (1988).

[6] see for example P. Cvitanović, *Physica* **D 51**, 138 (1991).

[7] Y. Ishii, "Towards the Kneading Theory for Lozi Attractors. I. Critical Sets and Pruning Fronts", Kyoto Univ. Math. Dept. preprint (Feb. 1994); "Towards the Kneading Theory for Lozi Attractors. II. A solution of the pruning front conjecture and partial monotonicity of the topological entropy", submitted to *Nonlinearity* (Apr. 1994).

[8] K.T. Hansen, *"Symbolic Dynamics in Chaotic Systems"*, Ph. D. thesis (University of Oslo 1993).

[9] K.T. Hansen, *CHAOS* **2**, 71 (1992); *Nonlinearity* **6**, 753 (1993); *Nonlinearity* **6**, 771 (1993).

[10] R. Lozi, *J. de Phys.* (Paris) **39**, Colloq. **C5**, 9 (1978).

[11] L. Bunimovich, *Funct. Anal. Appl.* **8**, 254 (1974); *Comm. Math. Phys.* **65**, 295 (1979).

[12] O. Biham and M. Kvale, *Phys. Rev.* **A 46**, 6334 (1992).

[13] L.A. Bunimovich, *CHAOS* **5**, 349 (1995).

[14] S. Smale, *Bull. Am. Math. Soc.* **73**, 747 (1967).

[15] B. Eckhardt, *J. Phys.* **A 20**, 5971 (1987).

[16] V.I. Arnold and A. Avez, *Ergodic Problems of Classical Mechanics* (Benjamin, New York 1968).

[17] Ya.G. Sinai, *Russ. Math. Surveys* **25**, 137 (1970).

[18] L. Bunimovich, *Sov. Phys. JETP* **62**, 842 (1985).

[19] L. Bunimovich and Y.G. Sinai, *Comm. Math. Phys.* **78**, 247 (1980).

[20] S. Akiyama and A. Koga, "Statistical Properties of Unstable Periodic Orbits in the stadium billiard", (Yamanashi Medical College preprint, Sept. 1994).

[21] P. Cvitanović and B. Eckhardt, *Nonlinearity* **6**, 277 (1993).

[22] E. Artin and B. Mazur, *Annals. Math.* **81**, 82 (1965).

[23] P. Grassberger, H. Kantz and U. Moening, *J. Phys.* **A 43**, 5217 (1989).

[24] D.H. Mayer, *Bull. Soc. Math. France* **104**, 195 (1976).

[25] R. Artuso, E. Aurell and P. Cvitanović, *Nonlinearity* **3**, 325 (1990).

[26] R. Artuso, E. Aurell and P. Cvitanović, *Nonlinearity* **3**, 361 (1990).

[27] J.D. Meiss, *CHAOS* **2**, 267 (1992); in *Quantum Chaos - Quantum Measurement*, P. Cvitanović, I. Percival, and A. Wirzba, eds. (Kluwer, Dordrecht, 1992).

Figure 11: The Poincaré section of the unstable manifold of the unstable period 2 cycle in the $a = 1.0$ stadium billiard drawn in the x (position along the boundary) and the incidence angle ϕ (outgoing angle to the normal) phase space for (a) the sidewall and (b) the semicircle. Both the stable and the unstable manifolds are drawn in (c) and (d) for the respective phase spaces.

Figure 12: The $a \to \infty$ Markov partition of the sidewall phase space I: a) $a = 5$, b) $a = 1$, c) $a = 0.5$.

PC: The second Fig. 15 is supposed to motivate the relation between the Markov graph and the well-ordered partition of the phase space/symbol plane; it says each node has its past and future, and Markov partition implements this in the symbol plane.

PC: replace table 1 by a figure with the tree.

Figure 13: The $a \to \infty$ Markov partition of the first semicircle bounce phase space II: a) $a = 5$, b) $a = 1$, c) $a = 0.5$. The empty regions are filled by the 2-nd or later bounces, Fig. 13.

Figure 14: The $a \to \infty$ Markov partition of the "not-first" semicircle bounce phase space III: a) $a = 5$, b) $a = 1$, c) $a = 0.5$.

Figure 15: The first level of the partition of the symbol planes (a) I; the vertical γ-axis is divided in two for the two possible future symbols $[.g]$ and $[.f]$: $0 \leq \gamma < 1/2$ corresponds to $[.g]$, and $1/2 \leq \gamma \leq 1$ corresponds to $[.f]$. The horizontal δ-axis is divided into five equal intervals for the five possible past symbols $[j.]$, $[h.]$, $[i.]$, $[k.]$, and $[f.]$, with the ordering of the five symbols the same as in the phase space I, Fig. 12. (b) II, (c) III.

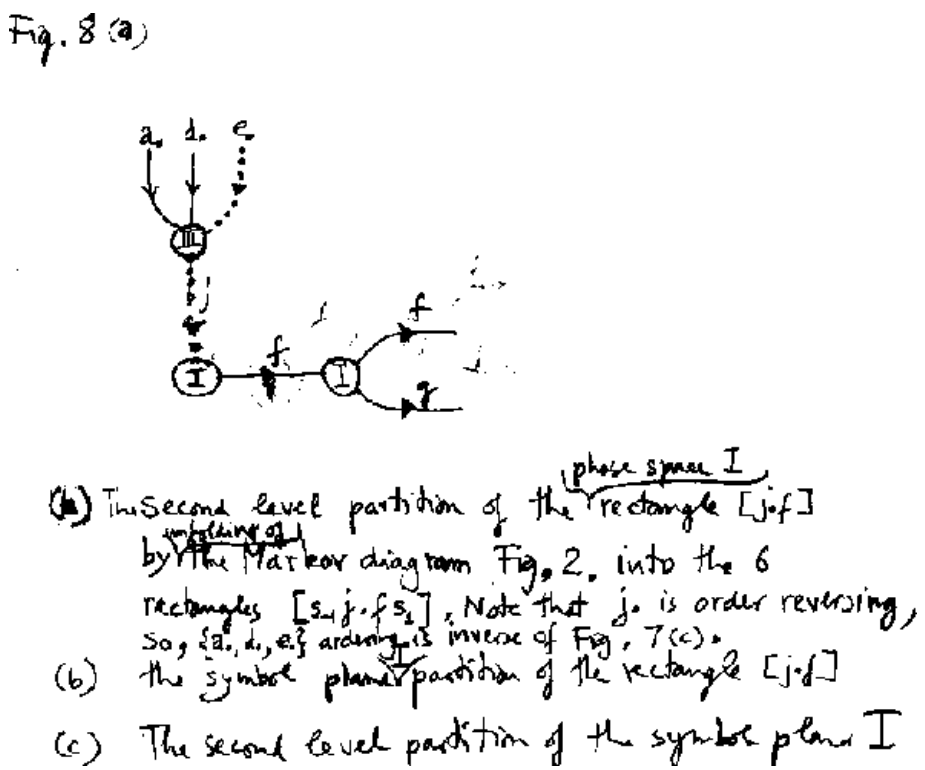

Figure 16: The second level partition of the phase space I rectangle $[j.f]$ into 6 rectangles $[s_{-1}j.fs_2]$. by unfolding of the Markov diagram of Fig. 9. Note that $j.$ is order-reversing, so the $\{a., d., e.\}$ ordering is inverse of Fig. 15(c). (b) The symbol plane I partition of the $[j.f]$. (c) The second level of the partition of the whole plane.

Figure 17: The pruning fronts in the symbol plane I for parameter (a) $a = 5$, (b) $a = 1$ and (c) $a = 0.5$.

Figure 18: The pruning front in the symbol plane II for parameter $a = 1$.

Figure 19: The pruning front in the symbol plane III for parameter $a = 1$.

Figure 20: Points in a few randomly initiated chaotic stadium trajectories in the symbol plane I for parameter (a) $a = 5$, (b) $a = 1$ and (c) $a = 0.5$. The primary forbidden regions, delineated by the pruning fronts of Fig. 17, together with their images and preimages, are never visited.

Figure 21: The pruning front in the symbol plane I for parameter $a = 1$, together with the second level partition lines of Fig. 16 (b). The approximate primary pruned region is shaded.

s	v
$[.g]$	0
$[.f]$	1
$[j.]$	$0 \quad (r)$
$[h.]$	$1 \quad (r)$
$[i.]$	2
$[k.]$	3
$[f.]$	4

s	v
$[.d]$	$0 \quad (r)$
$[.h]$	$1 \quad (r)$
$[.b]$	2
$[.i]$	3
$[.e]$	4
$[b.]$	0
$[c.]$	1
$[g.]$	2

s	v
$[.k]$	$0 \quad (r)$
$[.c]$	$1 \quad (r)$
$[.j]$	2
$[.a]$	3
$[e.]$	$0 \quad (r)$
$[d.]$	1
$[a.]$	2

Table 1: Definition of the well-ordered symbols v_t from the symbols s_t for the three phase spaces I, II and III. The letter r indicates that this symbol reverses the ordering of the following (or preceding) symbols.

10 Flotsam

Symbolic dynamics is closely related to Markov partitions of the dynamical phase space; an alphabet labels the distinct regions of the phase space, and a Markov graph or a transition matrix indicates how these are interconnected by the dynamics.

If we use the definition of the Poincaré section as in Fig. 5 and if the Poincaré section for the next semicircle is obtained by rotatatin this one by 180^0 and translating into the appropriate tile, the future itenerary conversion to well-ordered symbols:

first step into future:
S_i increases with ϕ_i and/or with x_i second step into future: x_{i+1}, R_i decreases with increasing ϕ_i and/or x_i ϕ_{i+1}, S_{i+1} decreases with increasing ϕ_i and/or x_i

from now on it is recursive, with R_{i+1}, S_{i+2} increasing with ϕ_i and/or x_i, and so on

past itenerary conversion to well-ordered:

first step into past: R_{i-1} decreases with ϕ_i and/or x_i x_{i+1}, S_{i-1} decreases with increasing ϕ_i and/or x_i second step into past: ϕ_{i+1}, R_{i-2} increases with increasing ϕ_i and/or x_i and so on.

10.1 1-step symbolic dynamics

The Markov graph consists of 3 nodes, corresponding to bounces either off the sidewall (I), off the semicircle as a first bounce in the semicircle (II), or off the semicircle as a second or later bounce (III), and the following list of links:

Starting from a sidewall, the trajectory hits either the opposite sidewall or a semicircle next

$$\begin{array}{lll} \mathrm{I} \xrightarrow{f} \mathrm{I} & & \text{sidewall} \\ \mathrm{I} \xrightarrow{g} \mathrm{II} & & \text{semicircle}\,. \end{array}$$

Having hit a semicircle once, the trajectory can hit the opposite semicircle, continue on the same semicircle (preserving or reversing the sense of the previous semicircle rotation), or hit either of the sidewalls (preserving or reversing the sense of the previous translation direc-

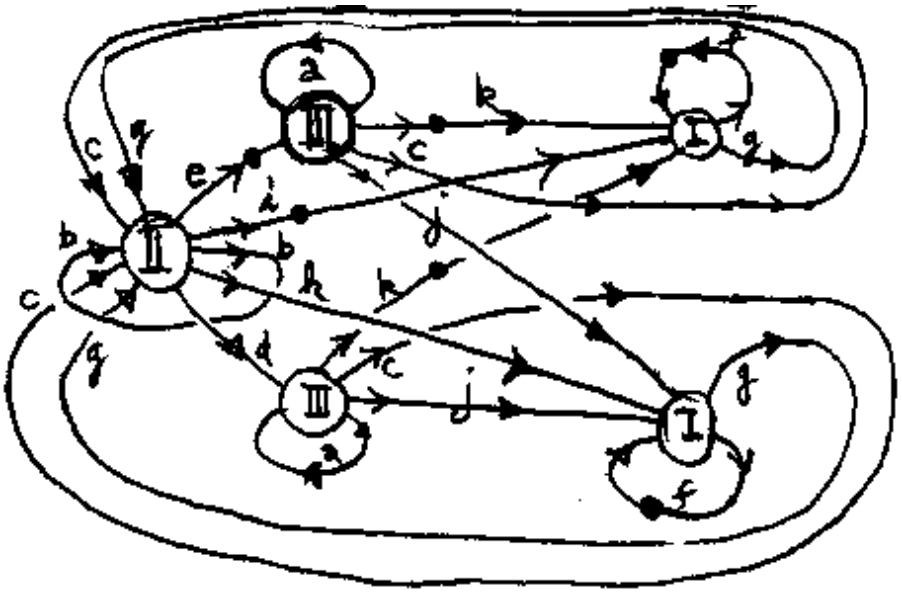

Figure 22: Markov diagram for the C_{2v} symmetric 1/4 stadium, 1-step symbolic dynamics.

tion):

II	$\stackrel{b}{\longrightarrow}$	II	fly across
II	$\stackrel{d}{\longrightarrow}$	III	semicircle, preserve sense of rotation
II	$\stackrel{e}{\longrightarrow}$	III	semicircle, reverse sense of rotation
II	$\stackrel{h}{\longrightarrow}$	I	sidewall, preserve sense of translation
II	$\stackrel{i}{\longrightarrow}$	I	sidewall, reverse sense of translation .

Finally, having hit a semicircle twice, the trajectory can hit the opposite semicircle, continue on the same semicircle (preserving the sense of rotation), or hit either of the sidewalls (preserving or reversing the sense of the previous translation direction):

III	$\stackrel{a}{\longrightarrow}$	III	continue around the semicircle
III	$\stackrel{c}{\longrightarrow}$	II	fly across
III	$\stackrel{j}{\longrightarrow}$	I	sidewall, preserve sense of translation
III	$\stackrel{k}{\longrightarrow}$	I	sidewall, reverse sense of translation .

Putting all this together, we obtain the 3-node Markov graph of Fig. 9, with the 11-letter alphabet $s_t \in \{a, b, c, d, \ldots, k\}$ labeling paths from one node to the next. There can be several topologically distinct paths connecting a pair of nodes.

10.2 Markov partitions

Partition I: corresponds to bounces off the sidewall, with a position $-a < x < a$ (with $x = 0$ on the center of the sidewall), and an outgoing angle $0 < \phi < \pi/2$. There are 5 ways to enter the node and 2 ways to leave. This yields a partition into 10 rectangles, Fig. 12:

The phase space partition I, Fig. 12, is drawn by noting that the five arrows going into the node I in Fig. 9 are $[j.]$, $[h.]$, $[i.]$, $[k.]$ and $[f.]$, and that the two outgoing arrows are $[.g]$ and $[.f]$. The partition border between $[.g]$ and $[.f]$ is given by the orbits bouncing straight into the singular point, and the partition border between $[f.]$ and $[k.]$ is given by orbits arriving directly from the singular point. The partition borders between $[k.]$ and $[i.]$ and between $[h.]$ and $[j.]$ are the given by orbits arriving at a point on the semicircle wall from the singular point and then bouncing once off this semicircle before reaching the sidewall. The partition border between $[i.]$ and $[h.]$ is a part of the unstable manifold of the hyperbolic period-2 cycle (dashed curve). Points on this partition border correspond to the orbits which hit the sidewall segment after having bounced an infinite number of times from one semicircle to the other.

Partition II: corresponds to a first bounce off the semicircle with a position $0 < x < \pi$ (with the two singular end points at $x = 0$, $x = \pi$) and an outgoing angle $x/2 < \phi < \pi/2+x/2$. There are 3 ways to enter the node and 5 ways to exit, yielding a partition of the phase space into 15 rectangles. Fig. 13. In the phase space partition II, Fig. 13, three arrows $[g.]$, $[c.]$, and $[b.]$ go into the node II in Fig. 9, and there are five outgoing arrows $[.d]$, $[.h]$, $[.b]$, $[.i]$, and $[.e]$. If $\phi < x/2$ or $\phi > \pi/2 + x/2$, then the previous bounce was off the same semicircle, *ie.* this bounce is not the first bounce off the semicircle, and thus does not belong to phase space II. The partition borders between the rectangles are given by orbits going into the singular point directly, or after one bounce in the other semicircle. The partition borders between the symbols $[.d]$ and $[.h]$ and between $[.i]$ and $[.e]$ are simply the straight lines $\phi = \pi/2 - x/2$, $\phi = \pi - x/2$. In addition to these partition borders we have drawn the first smooth fold of the unstable manifold of the 2-cycle which has a point in the center of this plane at $x = \pi/2$, $\phi = \pi/2$. This curve (dashed line in Fig. 13) determines the orientation of a bounce and hence the fundamental domain.

PC: dropped this: Each symbol string $[s_0.s_1]$ is here drawn in two disconnected rectangles, with any two rectangles with the same labeling symmetric to each other.

Partition III: corresponds to a second or later bounce off the semicircle with a position $0 < x < \pi$, and an outgoing angle $0 < \phi < x/2$.

PC: changed from $[s_{t-1}.s_t]$

There are 3 ways to enter this node and 4 ways to exit, yielding a partition into 12 rectangles, Fig. 14.

In the phase space III, Fig. 14, there are three arrows $[a.]$, $[d.]$, and $[e.]$ going into the node in Fig. 9, and there are four outgoing arrows $[.a]$, $[.j]$, $[.c]$, and $[.k]$. If $x/2 < \phi < \pi/2 + x/2$ the previous bounce was not off the same semicircle, so such points belong to the phase space II. We then only have to look at $\phi < x/2$. The partition border separating $[a.]$ and $[d.]$ is the line $\phi = x/4$. The border separating $[d.]$ and $[e.]$ is one fold of the unstable manifold of the horizontal 2-cycle (dashed curve). This particular fold consist of all orbits which bounce back and forth between the two semicircles and then twice off the same semicircle wall, with the second bounce off the semicircle yielding a point in the fold. The border separating $[.a]$ and $[.j]$ is the line $\phi = \pi/2 - x/2$, and the borders separating $[.j]$, $[.c]$ and $[.k]$ correspond to the orbits bouncing straight into a singular point of the other semicircle.

In the infinite length $a \to \infty$ limit this partitioning of the stadium phase space is complete. As a decreases the rectangles lose orbits, and for sufficiently small parameter values some rectangles may be completely lost. This loss of orbits will be described below in terms of the pruning front.

The borders between the rectangles drawn in Figs. 12, 13 and 14 are of two types: (a) solid line: partition borders generated by orbits with a given finite intenerary which end in or originate from the singular point on the stadium wall. (b) dashed line: partition borders generated by orbits with a specific intenerary belonging to the stable or unstable manifold of the hyperbolic period-2 cycle. These curves partition the phase space into rectangles labeled by the three $[s_0.s_1]$ pairs, 10+15+12=37 rectangles in all.

PC: changed from $[s_{t-1}.s_t]$

The rectangles map into each other with the partition borders mapping into the partition borders, and in the $a \to \infty$ limit the borders are invariant manifolds, as required for a complete Markov partition.

As the length a decreases, the rectangles change, and at $a = 1$ the rectangle $[j.f]$ in phase space I and the rectangle $[a.k]$ in phase space III disappear completely. This is the bifurcation point for the $\overline{011022} = \overline{cea}$ cycle and the associated family of orbits (see ref.[9]) which includes the orbits $\overline{234010} = \overline{jfgdce}$ and $\overline{113020} = \overline{akgdce}$ with points in these rectangles. Also other rectangles partly disappear and become smaller. This is not easily seen in the phase space figures because there the metric area might sometimes grow even while the number of orbits of given length within the rectangle decreases.

PC: replace $\overline{011022}$, $\overline{234010}$, $\overline{113020}$ by the appropriate 1/4 stadium unfolded symbols!